J Biol Inorg Chem
DOI 10.1007/s00775-011-0871-y

ORIGINAL PAPER

Evaluation of novel ^{99m}Tc(I)-labeled homobivalent α-melanocyte-stimulating hormone analogs for melanocortin-1 receptor targeting

Maurício Morais · Paula D. Raposinho · Maria Cristina Oliveira · João D. G. Correia · Isabel Santos

Received: 21 October 2011 / Accepted: 18 December 2011

Abstract Aiming to apply the multivalency concept to melanoma imaging, we have assessed the in vivo melanocortin type 1 receptor (MC1R)-targeting properties of ^{99m}Tc(I)-labeled homobivalent peptide conjugates which contain copies of the α-melanocyte-stimulating hormone (α-MSH) analog [Ac-Nle^4, Asp^5, D-Phe^7, Lys^{11}]α-MSH$_{4–11}$ separated by linkers of different length (**L^2** nine atoms and **L^3** 14 atoms). The MC1R-binding affinity of **L^2** and **L^3** is significantly higher than that of the monovalent conjugate **L^1**. Metallation of these conjugates yielded the complexes *fac*-[M(CO)$_3$(k^3-L)]$^+$ (M is ^{99m}Tc/Re; **1/1a**, L is **L^1**; **2/2a**, L is **L^2**; **3/3a**, L is **L^3**), with IC$_{50}$ values in the subnanomolar and nanomolar range. The MC1R-mediated internalization of **2** and **3** is higher than that of **1** in B16F1 melanoma cells. Biodistribution studies in melanoma-bearing mice have shown low nonspecific accumulation with a tumor uptake that correlates with IC$_{50}$ values. However, no correlation between tumor uptake and valency was found. Nevertheless, **2** displayed the highest tumor retention, and the best tumor to nontarget organ ratios.

Keywords Melanoma · α-Melanocyte-stimulating hormone · Melanocortin-1 receptor · Technetium-99m · Peptides

M. Morais · P. D. Raposinho · M. C. Oliveira · J. D. G. Correia · I. Santos (✉)
Unidade de Ciências Químicas e Radiofarmacêuticas, ITN, Estrada Nacional 10,
2686-953 Sacavém, Portugal
e-mail: isantos@itn.pt

Introduction

The overexpression of peptide receptors in a variety of human cancer cells led to the design, synthesis, and biological evaluation of various receptor-specific peptide-based radioactive tools for single photon emission computed tomography (γ-emitter radionuclides), positron emission tomography (β^+-emitter radionuclides), or targeted radionuclide therapy (β^- or α particles) [1–3]. Melanoma is the most aggressive type of skin cancer mainly owing to its high metastatic potential and resistance to current cytotoxic agents [4–7]. Improvement of patient survival relies mostly on an early diagnosis in combination with an accurate staging of disease extension [4–7]. Therefore, the design of novel radioactive compounds for melanoma imaging or therapy became a quite attractive approach for the management of both metastatic and nonmetastatic melanoma patients [1, 8]. The melanocortin type 1 receptor (MC1R) is overexpressed in both melanotic and amelanotic murine and human melanoma cells, and has been explored as a specific molecular target for melanoma detection [8–18]. α-Melanocyte-stimulating hormone (α-MSH), a linear tridecapeptide (Ac-Ser^1-Tyr^2-Ser^3-Met^4-Glu^5-His^6-Phe^7-Arg^8-Trp^9-Gly^{10}-Lys^{11}-Pro^{12}-Val^{13}-NH$_2$), is the native ligand that binds to the five subtypes of melanocortin receptors (MC1R–MC5R) [19–21]. Structure–bioactivity studies have shown that the minimal sequence His-Phe-Arg-Trp in α-MSH is sufficient for receptor recognition [19–21]. The replacement of Met^4 and Phe^7 by Nle^4 and D-Phe^7 led to the potent α-MSH analog (Nle^4, D-Phe^7)–α-MSH (NDP–MSH) with subnanomolar receptor affinity and resistance to enzymatic degradation [19–21]. Among the linear α-MSH analogs explored for melanoma imaging, [Ac-Nle^4, Asp^5, D-Phe^7, Lys^{11}]α-MSH$_{4–11}$ (NAPamide) has been one of the most studied for positron emission tomography (^{68}Ga, ^{64}Cu)

Published online: 29 January 2012

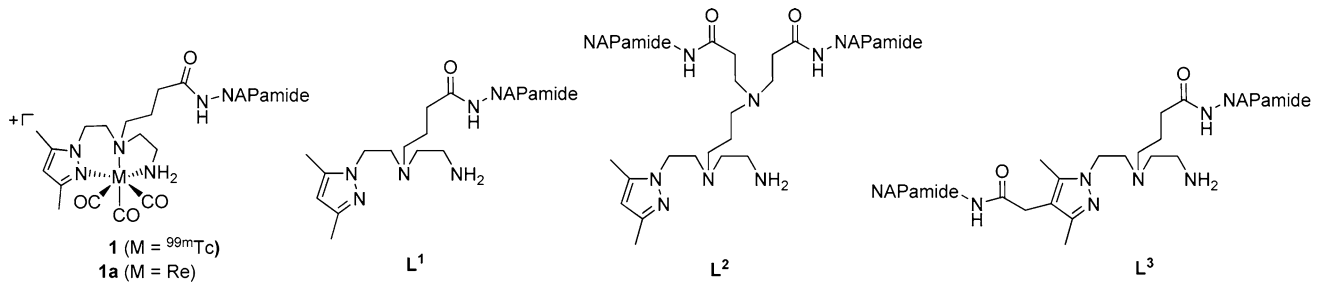

Fig. 1 *fac*-[M(CO)$_3$-(k^3-**L^1**)] complexes **1/1a** (M is ^{99m}Tc/Re) and [Ac-Nle^4, Asp^5, D-Phe7, Lys^{11}]α-MSH$_{4–11}$ (*NAPamide*; where α-MSH is α-melanocyte-stimulating hormone) conjugates **L^1**–**L^3**

or single photon emission computed tomography (^{111}In, ^{67}Ga, ^{99m}Tc) imaging [11, 12, 14, 18, 22].

The multivalent approach, which is characterized by the use of constructs displaying multiple copies of a molecular recognition element, aims to enhance the affinity for a specific target by different mechanisms. Such an approach when applied to the design of nuclear probes intends to amplify the imaging signal, a crucial issue for a more effective targeted tumor imaging [1, 23–25]. The most successful examples of this approach were achieved with radiolabeled multimeric cyclic RGD peptides, where an increase in peptide multiplicity significantly enhanced the integrin $\alpha_v\beta_3$ binding affinity with improvement of the tumor-targeting ability [24, 26–31].

The first examples of α-MSH multivalent constructs consisted of several α-MSH molecules coupled to albumin, thyroglobulin, and tobacco mosaic virus, which displayed a 1,500-fold higher potency than α-MSH alone [32, 33]. Further structure–bioactivity studies have demonstrated that enhanced binding affinity could also be achieved with bivalent constructs [34, 35]. The effect of flexible [poly(ethylene glycol)] or rigid (phenyl, biphenyl, and phenylnaphthyl) linkers, with variable length, on the affinity of short bivalent α-MSH constructs has also been evaluated [34, 35]. Despite not being conclusive about the optimal linker to span two G-protein-coupled receptors, the in vitro studies have shown that bivalent ligands display higher activity than the monovalent ligand (eightfold to 22.3-fold) [35]. This effect was even more pronounced for monovalent compounds with low binding affinity [34]. In spite of the research efforts towards the preparation of bivalent α-MSH constructs with enhanced affinity, few attempts have been made to evaluate their in vivo MC1R-targeting properties. Indeed, to the best of our knowledge, there have only been a few reports on the in vivo evaluation of radiolabeled homobivalent α-MSH conjugates [36, 37]. The conjugation of α-MSH analogs to bifunctional chelators such as diethylenetriaminepentaacetic acid and 1,4,7,10-tetraazacyclododecane-1,4,7,10-tetraacetic acid (DOTA) gave peptide conjugates with enhanced binding affinity compared with the monovalent counterparts [36, 37]. However, the [^{111}In-DOTA]-labeled homodimeric peptide conjugates exhibited low tumor uptake with unfavorable tumor to normal tissue ratios in B16F1 melanoma-bearing mice [37]. Most recently, the encouraging results obtained with the monovalent compound *fac*-[^{99m}Tc(CO)$_3$-(k^3-**L^1**)] (**1**, Fig. 1), which exhibited moderate MC1R tumor uptake and promising excretion kinetics in B16F1 melanoma-bearing mice [17], prompted us to explore the multivalency concept.

Therefore, aiming at the design of novel radioactive probes with improved MC1R-targeting properties and superior tumor to normal tissue ratios, we report herein on the synthesis and characterization of novel homobivalent NAPamide conjugates (**L^2** and **L^3**) bearing pyrazolyl-diamine-containing chelating units (Fig. 1) and on their (radio)metallation with the organometallic core *fac*-[M(CO)$_3$]$^+$ (M is ^{99m}Tc, Re). The in vitro and in vivo MC1R-targeting properties of the bivalent radiometallated peptides are also reported and compared with those of the monovalent (radio)metallated peptides **1/1a** (M is ^{99m}Tc/Re) depicted in Fig. 1.

Materials and methods

Materials and instrumentation

The α-MSH analog NDP–MSH was purchased from Neosystem (Strasbourg, France). Bovine serum albumin (BSA) and trifluoroacetic acid (TFA) were purchased from Sigma. Dulbecco's modified Eagle's medium (DMEM) containing GlutaMax I, fetal bovine serum, penicillin/streptomycin antibiotic solution, trypsin–EDTA, and phosphate-buffered saline (PBS) pH 7.2 were all from Gibco–Invitrogen (Alfagene, Lisbon, Portugal). The linear peptide NAPamide was synthesized using the usual continuous flow technology and the 9-fluorenylmethoxycarbonyl (Fmoc) strategy on a CEM 12-channel automated peptide synthesizer. Fmoc-amino acids were purchased from CEM. Fmoc-Lys(methyltrityl), the acid-labile Sieber resin, and 2-(7-aza-1*H*-benzotriazole-1-yl)-1,1,3,3-tetramethyluronium

hexafluorophosphate (HATU) were purchased from Novabiochem (Merck, Lisbon, Portugal). 4-((2-(*tert*-Butoxycarbonylamino)ethyl)(2-(3,5-dimethyl-1*H*-pyrazol-1-yl)ethyl) amino)butanoic acid [pz(Boc)(CO_2H)], *tert*-butyl 2-((3-aminopropyl)(2-(3,5-dimethyl-1*H*-pyrazol-1-yl)ethyl)amino) ethylcarbamate [pz(Boc)(NH_2)], *N*-*tert*-butyloxycarbonyl-1,2-ethylenediamine (Boc-NHCH_2CH_2NH_2), and 2-(1-(2-((2-(*tert*-butoxycarbonylamino)ethyl)(4-ethoxy-4-oxobutyl) amino)ethyl)-3,5-dimethyl-1*H*-pyrazol-4-yl)acetic acid [pz(Boc)(CO_2H)(CO_2Et)-B] were prepared as described elsewhere [38–41]. ^{1}H and ^{13}C NMR spectra were recorded with a Varian Unity 300 MHz spectrometer at room temperature. ^{1}H and ^{13}C chemical shifts were referenced with the residual solvent resonances relative to tetramethylsilane. The spectra were assigned on the basis of 2D experiments (^{1}H–^{1}H correlation spectroscopy). Assignments of the ^{1}H and ^{13}C NMR peaks are given in accordance with the identification system shown in Scheme 1. All other chemicals not specified were purchased from Aldrich. Electrospray ionization mass spectrometry (ESI–MS) was conducted with a Bruker HCT (Germany) electrospray ionization quadrupole ion trap mass spectrometer. Na[^{99m}TcO_4] was eluted from a ^{99}Mo/^{99m}Tc generator, using 0.9% saline. An IsoLink® kit (Mallinckrodt-Covidien, Petten, The Netherlands) was used to prepare the radioactive precursor *fac*-[^{99m}Tc(CO)$_3$(H_2O)$_3$]$^{+}$ as described elsewhere [39, 40, 42]. The synthon *fac*-[Re(CO)$_3$(H_2O)$_3$]Br was also prepared according to a method described previously [43]. No-carrier added sodium [^{125}I]-iodide (17.4 Ci/mg) in NaOH (0.1 M) was obtained from PerkinElmer.

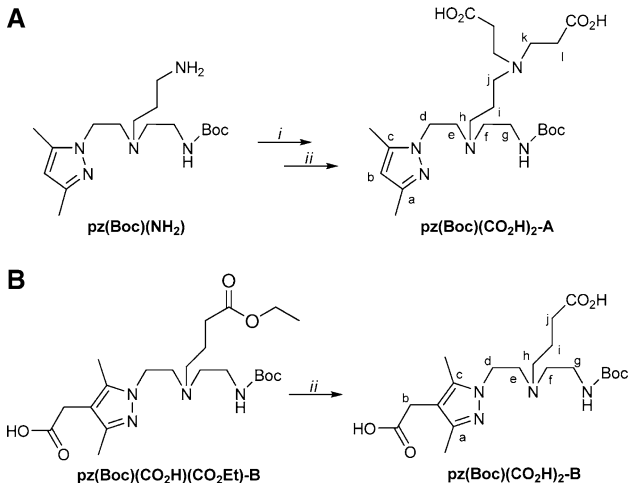

Scheme 1 Synthesis of pz(Boc)(CO_2H)$_2$-A (**a**) and pz(Boc)(CO_2H)$_2$-B (**b**). *i* CH_2CHCO_2Me, MeOH; *ii* NaOH, tetrahydrofuran/H_2O. *Boc* *tert*-butyloxycarbonyl

Chromatographic systems

High-performance liquid chromatography (HPLC) analyses were performed with a PerkinElmer liquid chromatography pump 200 coupled to a Shimadzu SPD 10AV UV–vis spectrometer and to a Berthold LB509 radiometric detector. Analytical control of the nonradioactive compounds was achieved using an analytical Macherey–Nagel C_{18} reversed-phase column (Nucleosil 100-10, 250 mm × 4 mm) with a flow rate of 1.0 mL min^{-1}, and purification of those compounds was achieved using a semipreparative Macherey–Nagel C_{18} reversed-phase column (Nucleosil 100-7, 250 mm × 8 mm) or a preparative Waters μ Bondapak C_{18} column (150 mm × 19 mm), the contents of which were eluted with a binary gradient system with a flow rate of 2.0 and 5.0 mL min^{-1} (gradients A–D), respectively. The absorbance was monitored at 220 and 280 nm. Analytical control and semipreparative purifications of the ^{99m}Tc(CO)$_3$-labeled α-MSH analogs were done on Hypersil octadecyl silica columns (250 mm × 4 mm, 10 μm; 250 mm × 8 mm, 10 μm), the contents of which were eluted with a binary gradient system with a flow rate of 1.0 mL min^{-1} (analytical) or 2.0 mL min^{-1} (gradient D), respectively.

Applied binary gradients

Gradient A (mobile phase A was aqueous 0.1% TFA and mobile phase B was MeOH): 0–3 min, 0% mobile phase B; 3–3.1 min, 0–25% mobile phase B; 3.1–9 min, 25% mobile phase B; 9–9.1 min, 25–34% mobile phase B; 9.1–20 min, 34–100% mobile phase B; 20–25 min, 100% mobile phase B; 25–25.1 min, 100–0% mobile phase B; 25.1–30 min, 0% mobile phase B.

Gradient B [mobile phase A was 0.1% TFA; mobile phase B was CH_3CN and 0.1% TFA]: 0–35 min, 70–100% mobile phase B; 35–37 min, 100% mobile phase B; 37–38 min, 100–70% mobile phase B; 38–40 min, 70% mobile phase B.

Gradient C (mobile phase A was TFA 0.1%; mobile phase B was CH_3CN and 0.1% TFA): 0–25 min, 50–100% mobile phase B; 25–35 min, 100% mobile phase B; 35–36 min, 100–50% mobile phase B; 36–40 min, 50% mobile phase B.

Gradient D (mobile phase A was 0.5% TFA; mobile phase B was CH_3CN and 0.5% TFA): 0–3 min, 0% mobile phase B; 3–3.1 min, 0–25% mobile phase B; 3.1–9 min, 25% mobile phase B; 9–9.1 min, 25–34% mobile phase B; 9.1–14.1 min, 34–100% mobile phase B; 14.1–19 min, 100% mobile phase B; 19–21 min, 100–0% mobile phase B; 21–30 min, 0% mobile phase B.

Synthesis of pyrazolyl-diamine chelators and rhenium complexes

Synthesis of methyl 8-(2-(3,5-dimethyl-1H-pyrazol-1-yl)ethyl)-12-(3-methoxy-3-oxopropyl)-2,2-dimethyl-4-oxo-3-oxa-5,8,12-triazapentadecan-15-oate

A solution of pz(Boc)(NH_2) (0.06 g, 0.17 mmol) in dry methanol was added dropwise to a cold methanolic solution (0 °C) of methyl acrylate (0.076 g, 0.88 mmol). After the mixture had been stirred overnight at room temperature, the solvent was evaporated, and the crude product was purified by column chromatography (silica gel, $CHCl_3$/MeOH 2.5–20%), giving methyl 8-(2-(3,5-dimethyl-1H-pyrazol-1-yl)ethyl)-12-(3-methoxy-3-oxopropyl)-2,2-dimethyl-4-oxo-3-oxa-5,8,12-triazapentadecan-15-oate [pz(Boc)(CO_2Me)$_2$-A] as a white solid. Yield: 71% (0.07 g, 0.13 mmol). ^{1}H NMR (300 MHz, $CDCl_3$): δ (ppm) = 5.75 [s, H(4)pz, 1H], 3.96 (t, CH_2^d, 2H), 3.64 (s, CH_3^m, 6H), 3.07 (d, CH_2^g, 2H), 2.76 (t, CH_2^k, 2H), 2.7 (t, CH_2^e, 2H), 2.49 (t, CH_2^f, 2H), 2.38 (t, $CH_2^{l,m}$, 4H), 2.29 (t, CH_2^h, 2H), 2.21, (s, CH_3pz, 3H), 2, 19 (s, CH_3pz, 3H), 1.48 (t, CH_2^i,2H), 1.42 (s, CH_3, 9H). ^{13}C NMR (75.3 MHz, D_2O): δ (ppm) = 171.7 (CO), 171.6 (CO), 160.1 (CO), 145.5 (C^c), 141.5 (C^a), 101.3 (C^b), 78.0 (C(CH_3)), 52.1 (C^f), 51.5 (C^e), 51.4 (C^h), 50.7 (C^j), 50.4 (C^m) 50.1 (C^k), 47.9 (C^d), 37.6 (C^g), 30.3 (C^l), 28.8 (C(CH_3)), 20.5 (C^i), 11.2 (CH_3pz), 10.1 (CH_3pz).

Synthesis of 12-(2-carboxyethyl)-8-(2-(3,5-dimethyl-1H-pyrazol-1-yl)ethyl)-2,2-dimethyl-4-oxo-3-oxa-5,8,12-triazapentadecan-15-oic acid

A solution of pz(Boc)(CO_2Me)$_2$-A (0.07 g, 0.13 mmol) and NaOH (0.055 g, 1.37 mmol) in H_2O/tetrahydrofuran (3 mL/3 mL) was refluxed overnight. After neutralization of the reaction solution with1 M HCl at 0 °C and evaporation of the solvent, the crude product obtained was purified with use of a Sep-Pack C_{18} cartridge (H_2O/MeOH 0–100%), giving 12-(2-carboxyethyl)-8-(2-(3,5-dimethyl-1*H*-pyrazol-1-yl)ethyl)-2,2-dimethyl-4-oxo-3-oxa-5,8,12-triazapentadecan-15-oic acid [pz(Boc)(CO_2H)$_2$-A] as a white solid. Yield: 75% (0.05 g; 0.1 mmol). ^{1}H NMR (300 MHz, D_2O): δ (ppm) = 5.78 [s, H(4)pz, 1H], 3.88 (t, CH_2^d, 2H), 3.1 (t, CH_2^k, 4H), 2.96 (t, CH_2^g, 2H), 2.79 (t, CH_2^e, 2H), 2.7 (t, CH_2^f, 2H), 2.41 (t, $CH_2^{l,\ j,\ h}$, 8H), 2.1 (s, CH_3pz, 3H), 1.99 (s, CH_3pz, 3H), 1.61 (t, CH_2^i, 2H), 1.25 (s, CH_3, 9H). ^{13}C NMR (75.3 MHz, D_2O): δ (ppm) = 179.7 (CO), 179.6 (CO), 160.1 (CO), 150.5 (C^c), 143.5 (C^a), 107.3 (C^b), 81.9 (C(CH_3)), 54.6 (C^f), 54.5 (C^e), 52.4 (C^h), 52.1 (C^j), 52.2 (C^k), 47.9 (C^d), 39.9 (C^g), 32.8 (C^l), 29.8 (C(CH_3)), 22.9 (C^i), 14.3 (CH_3pz), 12.4 (CH_3pz). Reversed-phase HPLC (RP-HPLC) (220 nm, gradient A): 99% (t_R = 17.4 min). ESI–MS (−) (*x*): 482.4 [M-H]$^+$, calcd. for $C_{23}H_{41}N_5O_6$ 483.3.

Synthesis of 4-((2-(tert-butoxycarbonylamino)ethyl)(2-(4-(carboxymethyl)-3,5-dimethyl-1H-pyrazol-1-yl)ethyl)amino)butanoic acid

A solution of pz(Boc)(CO_2H)(CO_2Et)-B [41] (0.20 g, 0.44 mmol) and excess NaOH (0.75 g, 2.10 mmol) in H_2O/tetrahydrofuran was refluxed overnight. After neutralization with HCl 1 M at 0 °C and evaporation of solvent, the obtained crude product was purified by solid phase extraction using Sep-Pack C_{18} cartridge (H_2O/MeOH 0–100%), giving 4-((2-(*tert*-butoxycarbonylamino)ethyl)(2-(4-(carboxymethyl)-3,5-dimethyl-1*H*-pyrazol-1-yl)ethyl)amino)butanoic acid [pz(Boc)(CO_2H)$_2$-B] as a white solid. Yield: 68% (0.14 g; 0.30 mmol). ^{1}H NMR (300 MHz, D_2O): δ (ppm) = 4.33 (t, CH_2^d, 2H), 3.57 (t, CH_2^e, 2H), 3.39 (s, CH_2^b, 2H), 3.30 (m, $CH_2^{f/h}$, 4H), 3.17 (t, CH_2^g, 2H), 2.34 (t, CH_2^j, 2H), 2.1 (s, CH_3pz, 3H), 2.03 (s, CH_3pz, 3H), 1.86 (t, CH_2^i, 2H), 1.24 (s, CH_3, 9H). ^{13}C NMR (75.3 MHz, D_2O): δ (ppm) = 189.8 (CO), 187.6 (CO), 165.1 (CO), 154.5 (C^c), 145.9 (C^a), 119.4 (Cpz), 88.8 [C(CH_3)], 60.2 (C^h), 59.7 (C^e), 59.2 (C^f), 52.4 (C^d), 44.1 (C^g), 42.3 (C^j), 38.8 (C^b), 34.8 [C(CH_3)], 29.5 (C^i), 17.7 (CH_3pz), 15.9 (CH_3pz). RP-HPLC (220 nm, gradient A): 99% (t_R = 16.7 min). ESI–MS (+) (*m*/*z*): 427.5 [M + H]$^+$, calcd. for $C_{20}H_{34}N_4O_6$ 426.4.

Synthesis of 4-((2-aminoethyl)(2-(4-(carboxymethyl)-3,5-dimethyl-1H-pyrazol-1-yl)ethyl)amino)butanoic acid

tert-Butyloxycarbonyl (Boc) deprotection of the intermediate compound pz(Boc)(CO_2H)$_2$-B (0.10 g, 0.20 mmol) with CH_2Cl_2/TFA (1 mL/3 mL) gave 4-((2-aminoethyl)(2-(4-(carboxymethyl)-3,5-dimethyl-1*H*-pyrazol-1-yl)ethyl)amino)butanoic acid [pz(CO_2H)$_2$-B] as a colorless oil after evaporation of the solvent. Yield: 92% (0.08 g, 0.19 mmol, calcd. for $C_{15}H_{26}N_4O_4$·TFA). ^{1}H NMR (300 MHz, D_2O): δ (ppm) = 4.42 (t, CH_2^d, 2H), 3.51 (t, CH_2^e, 2H), 3.40 (m, CH_2^f, 2H), 3.32 (s, CH_2^b, 2H), 3.23 (m, CH_2^g, 2H), 3.09 (m, CH_2^j, 2H), 2.72 (t, CH_2^h, 2H), 2.06 (s, CH_3pz, 3H), 1.99 (s, CH_3pz, 3H), 1.77 (m, CH_2^i, 2H). ^{13}C NMR (75.3 MHz, D_2O): δ (ppm) = 178.2 (CO), 176.9 (CO), 165.4 (q, CF_3COO^-), 149.4 (C^c), 145.5 (C^a), 118.4 (q, CF_3COO^-), 114.1 (pz), 54.4 (CH_2), 53.3 (CH_2), 51.5 (CH_2), 44.2 (CH_2), 35.5 (CH_2), 31.7 (CH_2), 29.8 (CH_2), 19.8 (CH_2), 11.5 (CH_3), 10.6 (CH_3). RP-HPLC (220 nm, gradient A): 99% (t_R = 10.5 min). ESI–MS (+) (*m*/*z*): 327.1 [M + H]$^+$, calcd. for $C_{15}H_{26}N_4O_4$ 326.2.

Synthesis of fac-[Re(CO)$_3$(k^3-pz(CO$_2$H))]$^+$

The synthesis of this complex has already been described but starting from a different synthon [44]. Briefly, pz(CO$_2$H) (0.05 mg, 0.131 mmol) reacted with the organometallic precursor [Re(CO)$_3$(H$_2$O)$_3$]Br (0.05 mg, 0.13 mmol) in refluxing water for 18 h. After evaporation of the solvent, the resulting residue was purified by preparative RP-HPLC (220 nm, gradient A). [Re(CO)$_3$(k^3-pz(CO$_2$H))]$^+$ was isolated as a colorless clear oil. Yield: 76% (50 mg, 0.08 mmol). ^{1}H NMR (300 MHz, D$_2$O): δ (ppm) = 6.01 (s, H^b, 1H), 5.07 (q br, NH, 1H), 4.33 (dd, CH^d, 1H), 4.07 (m, CH$^{d'}$, 1H), 3.62 (s br, NH, 1H), 3.50 (m, CH^j, 1H), 3.37 (m, CH$^{j'}$ + CH^e, 2H), 3.05 (s br, CH^g, 1H), 2.72 (d, CH^f + CH$^{f'}$, 2H), 2.54 (t br, CH$^{e'}$, 1H), 2.37 (m br, CH$^{g'}$, 1H), 2.33 (t, CH^h + CH$^{h'}$, 2H), 2.24 (s, CH$_3$pz, 3H), 2.14 (s, CH$_3$pz, 3H), 2.04 (m, CH^i, 1H), 1.88 (m, 1H, CH$^{i'}$). ^{13}C NMR (75 MHz, D$_2$O): δ (ppm) = 196.6 (C≡O), 196.2 (C≡O), 196.1 (C≡O), 179.8 (C=O), 155.7 (Cpz), 146.3 (Cpz), 109.8 (Cpz), 67.8 (C^j), 63.2 (C^f), 54.5 (C^e), 49.1 (C^d), 44.2 (C^g), 33.1 (C^h), 21.5 (C^i), 17.3 (CH$_3$pz), 12.9 (CH$_3$pz). RP-HPLC (220 nm, gradient A): 99% (t_R = 18.3 min). ESI–MS (+) (*m*/*z*): 597.0 [M + H]$^+$, calcd. for C$_{18}$H$_{29}$N$_4$O$_7$Re 599.6.

Synthesis of fac-[Re(CO)$_3$(k^3-pz(CO$_2$H)$_2$-A)]$^+$

The preparation of the rhenium complex was achieved after two steps. In the first step, the Boc protecting group was removed from the amino group of pz(Boc)(CO$_2$Me)$_2$-A with a dilute solution of TFA. Briefly, pz(Boc)(CO$_2$Me)$_2$-A (0.07 g, 0.13 mmol) was suspended in a solution (5 mL) of TFA (5%TFA/CH$_2$Cl$_2$) and the reaction mixture was stirred at room temperature for 3 h. After evaporation of the solvent, pz(CO$_2$Me)$_2$-A was obtained as a colorless oil. Yield: 88% (0.05 g, 0.12 mmol). The compound was briefly characterized by ^{1}H NMR spectroscopy (300 MHz, D$_2$O): δ (ppm) = 5.58 [s, H(4)pz, 1H], 4.27 (t, CH$_2^d$, 2H), 3.2 (s, CH$_3^m$, 6H), 2.96 (t, CH$_2^{e+k}$, 6H), 2.59–2.51 (m, CH$_2^{g+j+h}$, 6H), 2.38 (t, CH$_2^l$, 4H), 2.29 (t, CH$_2^f$, 2H), 1.77 (s, CH$_3$pz, 3H), 1.69 (s, CH$_3$pz, 3H), 1.39 (t, CH$_2^i$, 2H). In the second step, the complex was prepared according to the method described earlier for *fac*-[Re(CO)$_3$(k^3-pz(CO$_2$H))]$^+$. The compound pz(CO$_2$Me)$_2$-A (0.05 g, 0.12 mmol) reacted with the organometallic precursor [Re(CO)$_3$(H$_2$O)$_3$]Br (0.06 g, 0.15 mmol) in refluxing water for 18 h. After solvent evaporation, the resulting residue was purified by preparative RP-HPLC (220 nm, gradient A). The complex [Re(CO)$_3$(k^3-pz(CO$_2$H)$_2$-A]$^+$ was isolated as a colorless clear oil. Yield: 53% (0.04 g, 0.06 mmol). IR (KBr, cm^{-1}): 2,033 s and 1,932 s (C≡O) and 1,684 s (C=O). ^{1}H NMR (300 MHz, D$_2$O): δ (ppm) = 6.07 (s, H^b, 1H), 5.12 (q br, NH, 1H), 4.39 (dd, CH^d, 1H), 4.17 (m, CH$^{d'}$, 1H), 3.70 (q br, NH, 1H), 3.59 (dd, CH^j, 1H), 3.47 (t, CH^k, 4H), 3.36 (m, CH$^{j'}$, 1H), 3.31 (dd, CH^e, 1H), 3.22 (t, CH^j, 2H), 3.08 (dd, CH^g, 1H), 2.85 (t, CH^l, 4H), 2.78 (s, CH$^{f+f'}$, 2H), 2.69 (m, CH$^{g'+e'}$, 2H), 2.48 (m, CH^i, 1H), 2.30 (s, CH$_3$pz, 3H), 2.19 (s, CH$_3$pz, 3H). ^{13}C NMR (75.3 MHz, D$_2$O): δ (ppm) = 197.1 (C≡O), 196.6 (C≡O), 195.4 (C≡O), 176.9 (C=O), 156.5 (C^c), 147.1 (C^a), 110.5 (C^b), 65.3 (C^j), 63.8 (C^f), 55.4 (C^e), 53.7 (C^h), 52.2 (C^k), 49.6 (C^d), 44.9 (C^g), 30.9 (C^l), 21.9 (C^i), 17.9 (CH$_3$pz), 12.5 (CH$_3$pz). RP-HPLC (220 nm, gradient A): 99% (t_R = 15.9 min). ESI–MS (+) (*m*/*z*): 654.3 [M + H]$^+$, calcd. for C$_{21}$H$_{34}$N$_5$O$_7$Re 654.3.

Synthesis of fac-[Re(CO)$_3$(k^3-pz(CO$_2$H)$_2$-B)]$^+$

The complex was prepared according to the method described earlier for *fac*-[Re(CO)$_3$(k^3-pz(CO$_2$H))]$^+$. Briefly, pz(CO$_2$H)$_2$-B (100 mg, 0.23 mmol) reacted with the organometallic precursor [Re(CO)$_3$(H$_2$O)$_3$]Br (91 mg, 0.23 mmol) in refluxing water for 18 h. After evaporation of solvent, the resulting residue was purified by preparative RP-HPLC (220 nm, gradient A). The complex [Re(CO)$_3$(k^3-pz(CO$_2$H)$_2$-B]$^+$ was isolated as a colorless clear oil. Yield: 83% (120 mg, 0.18 mmol, calcd. for C$_{18}$H$_{29}$N$_4$O$_7$Re·TFA). IR (KBr, cm^{-1}): 2,028 and 1,927 s (C≡O) and 1,686 s (C=O). ^{1}H NMR (300 MHz, D$_2$O): δ (ppm) = 5.03 (br m, NH, 1H), 4.33 (dd, CH^d, 1H), 4.07 (dd, CH$^{d'}$, 1H), 3.61 (m, NH, 1H), 3.46 (m, CH^j, 1H), 3.38 (s, CH$_2^b$, 2H), 3.33 (m, CH^e + CH$^{j'}$, 2H), 3.03 (br dd, CH^g, 1H), 2.73 (br m, CH$_2^f$, 2H), 2.53 (m, CH$_2^{e'}$, 1H), 2.40 (m, CH$^{g'}$, 1H), 2.29 (t, CH^h, 2H), 2.18 (s, CH$_3$pz, 3H), 2.07 (s, CH$_3$pz, 3H), 1.96 (m, CH^i, 1H), 1.85 (m, CH$^{i'}$, 1H). ^{13}C NMR (75.3 MHz, D$_2$O): δ (ppm) = 196.3 (C≡O), 195.8 (C≡O), 194.8 (C≡O), 179.2 (C=O), 177.6 (C=O), 164.8 (q, CF$_3$COO$^-$), 154.4 (C^c), 144.7 (C^a), 118.2 (q, CF$_3$COO$^-$), 113.38 (pz), 67.4 (C^j), 62.9 (C^f), 54.2 (C^e), 49.1 (C^d), 44.0 (C^g), 32.6 (C^h), 30.5 (C^b), 21.1 (C^i), 15.4 (CH$_3$pz), 11,2 (CH$_3$pz). RP-HPLC (220 nm, gradient A): 99% (t_R = 17.5 min). ESI–MS (+) (*m*/*z*): 597.0 [M + H]$^+$, calcd. for C$_{18}$H$_{29}$N$_4$O$_7$Re 599.6.

Peptide synthesis

The fully protected α-MSH analog NAPamide was prepared by Fmoc-based solid phase peptide synthesis in a CEM 12-channel automated peptide synthesizer, using Sieber amide resin and the methyltrityl protecting group for the ε-amino group of Lys^{11}. After a one-pot reaction under mild acidic conditions (1% TFA/CH$_2$Cl$_2$) for selective removal of the methyltrityl group and peptide cleavage from the resin, the solution was concentrated to 5% of the initial volume and a white solid was precipitated with water in an ice bath. The crude product was washed consecutively with

water (three times), 5% aqueous $NaHCO_3$ (twice), water (three times), 0.05 M $KHSO_4$ (twice), and water (six times) and lyophilized. The crude peptide was dissolved in CH_3CN and purification of the partially protected NAPamide (Pp-NAPamide) was performed by semipreparative HPLC (220 nm, gradient B). After evaporation of the solvent, the partially deprotected α-MSH analog was obtained as a white solid. RP-HPLC (220 nm, gradient C): 99% (t_R = 19.4 min). ESI–MS (+) (*m*/*z*): 897 $[M + CH_3CN + 2H]^{2+}$, calcd. for $C_{93}H_{120}N_{16}O_{16}S$ 1,748.9.

Synthesis of the NAPamide conjugates $\mathbf{L^1}$–$\mathbf{L^3}$ and metallated derivatives **1a**–**3a**

A solution of Pp-NAPamide (2.5 equiv relative to each carboxylic group) in *N*,*N*-diisopropylethylamine (DIPEA) (20 μL)/dimethylformamide (250 μL) was added to the Boc-protected bifunctional chelators pz(Boc)(CO_2H), pz(Boc)$(CO_2H)_2$-A, and pz(Boc)$(CO_2H)_2$-B or rhenium precursors (*fac*-[Re$(CO)_3(k^3$-pz$(CO_2H))]^+$, *fac*-[Re$(CO)_3$ $(k^3$-pz-$(CO_2H)_2$-A)$]^+$, and *fac*-[Re$(CO)_3(k^3$-pz-$(CO_2H)_2$-B$)]^+$) preincubated for 30 min with HATU (1.2 equiv relative to each carboxylic group) in dimethylformamide. The pH was adjusted to 7–8 with DIPEA and the reaction mixtures were left to stir at room temperature for 3 h. The conjugation of Pp-NAPamide to pz(Boc)$(CO_2H)_2$-B was achieved after three cycles of microwave irradiation (40 W, 75 °C, 5 min).

The reaction mixtures were purified by semipreparative RP-HPLC (220 nm, gradient C). After evaporation of the solvent, the compounds were deprotected with a standard cocktail mixture (95% TFA, 2.5% triisopropylsilane, 2.5% H_2O) and precipitated with ice-cold diethyl ether. All compounds were lyophilized, and characterized by ESI–MS.

Radiolabeling with ^{99m}Tc(I)

The precursor *fac*-$[^{99m}Tc(CO)_3(H_2O)_3]^+$ was prepared by addition of Na$[^{99m}TcO_4]$ to an Isolink® kit (Covidien-Mallinckrodt) following a described procedure, and its radiochemical purity was checked by RP-HPLC [16–18, 39, 40, 44]. Compounds **2** and **3** were obtained by reacting $\mathbf{L^2}$ and $\mathbf{L^3}$ with *fac*-$[^{99m}Tc(CO)_3(H_2O)_3]^+$. Briefly, a solution of *fac*-$[^{99m}Tc(CO)_3(H_2O)_3]^+$ (900 μL) was added to a capped vial, previously flushed with N_2, containing $\mathbf{L^2}$ or $\mathbf{L^3}$ (100 μL, 5×10^{-4} M). The mixture reacted for 30 min at 100 °C, and the radiochemical purity of **2** and **3** was checked by RP-HPLC, using an analytical C_{18} reversed-phase column. The radiolabeled compound was purified by semipreparative RP-HPLC (gradient D). The activity corresponding to the $^{99m}Tc(CO)_3$ homodimeric conjugates was collected in a Falcon flask (50 mL) containing a 0.2% BSA solution in PBS (200 μL) for biodistribution and internalization studies. The solutions were concentrated to a final volume of 200 μL under a nitrogen stream, and the product was checked by analytical RP-HPLC to confirm its purity and stability after purification and evaporation. The Specific activity was 32.5 mCi/μg for **2** and 33.9 mCi/μg for **3**.

Partition coefficient

The partition coefficient was evaluated by the "shake-flask" method [45]. The radioconjugate was added to a mixture of octanol (1 mL) and 0.1 M PBS pH 7.4 (1 mL) which had been previously saturated with each other by stirring. This mixture was vortexed and centrifuged (3,000 rpm, 10 min) to allow phase separation. Aliquots of both octanol and PBS were counted in a γ-counter. The partition coefficient ($P_{o/w}$) was calculated by dividing the counts in the octanol phase by those in the buffer, and the results were expressed as log $P_{o/w} \pm$ the standard deviation.

Cysteine and histidine challenge

Aliquots of the ^{99m}Tc(I) complexes (100 μL) were added to 5×10^{-3} M cysteine or histidine solutions in PBS pH 7.4 (400 μL). The resulting solutions were incubated at 37 °C for 24 h and analyzed by analytical RP-HPLC using the method described in "Chromatographic systems."

In vitro stability

The in vitro stability of the radiopeptides was determined in aliquots of fresh human plasma obtained from a healthy volunteer. The volunteer was recruited and asked to provide informed consent. The ^{99m}Tc-labeled complex (100 μL, approximately 10 MBq) was added to fresh human plasma (1 mL), and the mixture was incubated at 37 °C. At appropriate time points (2, 4, and 6 h), 100-μL aliquots (in duplicate) were sampled and treated with 200 μL of ethanol to precipitate the proteins. Samples were centrifuged at 3,000 rpm for 15 min at 4 °C, and the supernatant was analyzed by HPLC. The stability of the radiolabeled conjugate in the solutions containing 0.2% BSA was checked by RP-HPLC using the chromatographic methods previously described and by instant thin-layer chromatography (5% 6 M HCl in MeOH).

Cell culture

B16F1 murine melanoma cells (ECACC, Porton Down, UK) were grown in DMEM containing GlutaMax I supplemented with 10% heat-inactivated fetal bovine serum and 1% penicillin/streptomycin antibiotic solution (all from

Gibco-Invitrogen). Cells were cultured in a humidified atmosphere of 95% air and 5% CO_2 at 37 °C (Heraeus, Germany), with the medium changed every other day. The cells were adherent in monolayers and, when confluent, were harvested from the cell culture flasks with trypsin–EDTA (Gibco-Invitrogen) and seeded further apart.

[^{125}I]NDP-MSH

Radioiodination of NDP-MSH with ^{125}I was performed by the chloramine-T method with small modifications [46]. Briefly, NDP-MSH (5 μg) in PBS 0.3 M (50 μL) was mixed with Na^{125}I (10 μL, 1.5 mCi) and then 10 μL of a chloramine-T solution in 0.3 M PBS (2 mg/mL) was added. After incubation for 5 min at room temperature, the reaction was stopped with 500 μL of dithiothreitol (20 mg/mL), and 100 μL of BSA (10 mg/mL) was added before purification. The mixture was loaded into a small reversed-phase cartridge (Sep-Pak C_{18}, Waters), the contents of which were eluted in a first step with TFA aqueous solution (0.1% TFA, 5 mL), followed by methanol (100%). The iodinated peptide was eluted with methanol and collected in fractions of 500 μL, which were stored at −20 °C.

Preceding each binding experiment, an additional purification was performed by RP-HPLC. Analytical purification of [^{125}I]NDP–MSH was achieved by analytical RP-HPLC with simultaneous radioactivity and UV detection (258 nm) on a Machery-Nagel column (250mm × 4 mm, 5 μm) using the following gradient: (mobile phase A, 0.1% TFA; mobile phase B, 140 mL CH_3CN + 60 mL H_2O + 200 μL concentrated TFA): 0–45 min, mobile phase A/mobile phase B 70:30 → 50:50; 40–55 min, 0:100; 55–56 min 0:100 → 70:30; 55–60 min, 70:30.

Competitive binding assay

The inhibitory concentration of 50% (IC_{50}) values for the α-MSH analogues were determined by competitive binding assays with [^{125}I]NDP-MSH in B16F1 melanoma cells. Cells were harvested, seeded into a 24-well cell culture plates (2×10^5 cells per well), and allowed to attach overnight. After they had been washed once with the binding medium [0.3 mL, DMEM with 25 mM *N*-(2-hydroxyethyl)piperazine-*N*′-ethanesulfonic acid and 0.2% BSA], the cells were incubated at room temperature (25 °C) for 2 h with the competitor peptide solution (0.1 mL), yielding a final concentration ranging from 1×10^{-5} to 1×10^{-12} M, and [^{125}I]NDP-MSH (50,000 cpm in 0.2 mL). The reaction medium was then removed, and the cells were washed twice with cold 0.01 M PBS pH 7.2 with 0.2% BSA (0.5 mL) and lysed with 1 M NaOH (0.5 mL) for 5 min. The radioactivity of the lysate was measured with a γ-counter. The competitive binding curves were obtained by plotting the percentage of [^{125}I]NDP-MSH bound to the cells versus the concentrations of displacing peptides. IC_{50} values for the peptides were calculated by using GraphPad Prism. All cell binding experiments were conducted in triplicate.

Internalization and cellular retention studies

Internalization assays of the radiopeptides were performed in B16F1 murine melanoma cells seeded at a density of 0.2 million per well in plates and allowed to attach overnight. The cells were incubated at room temperature or 37 °C for a period of 5 min to 4 h with about 200,000 cpm of the conjugate in 0.5 mL of assay medium [DMEM with 25 mM *N*-(2-hydroxyethyl)piperazine-*N*-ethanesulfonic acid and 0.2% BSA]. Incubation was terminated by washing the cells with ice-cold assay medium. Cell-surface-bound radioligand was removed by two steps of acid wash (50 mM glycine, HCl/100 mM NaCl, pH 2.8) at room temperature for 5 min. The pH was neutralized with cold PBS with 0.2% BSA, and subsequently the cells were lysed by 10 min incubation with 1 M NaOH at 37 °C to determine internalized radioligand. For assessing the specific MC1R-mediated uptake and internalization, a parallel study was performed using the potent agonist NDP–MSH (3.5 μg per well) to block the MC1Rs. The cellular retention properties of the internalized radioconjugates were determined by incubating B16F1 cells with the radiolabeled compound for 3 h at 37 °C, washing them with cold assay medium, removing the membrane-bound radioactivity with acid buffer wash, and monitoring the radioactivity released into the culture medium (0.5 mL) at 37 °C. At different time points over a 4-h incubation period, the radioactivity in the medium and that in the cells were separately collected and counted.

Biodistribution

All animal experiments were performed in compliance with national and European regulations for animal treatment. The animals were housed in a temperature- and humidity-controlled room with a 12 h light/12 h dark schedule. Biodistribution of the radiopeptides was performed in melanoma-bearing C57BL/6 female mice (8–10 weeks old). The mice had previously been implanted subcutaneously with 1×10^6 B16F1 cells to generate a primary skin melanoma. Ten to 12 days after the inoculation, tumors reached a weight of 0.2–1 g.

Radiolabeled complex (2.6–3.7 GBq) diluted in 100 μL of PBS pH 7.2 was intravenously injected into the retro-orbital sinus of the mice. The mice ($n = 3$–5 per time point) were killed by cervical dislocation at 1 and 4 h after injection. The dose administered and the radioactivity in

the killed animals were measured using a dose calibrator (Curiemeter IGC-3, Aloka, Tokyo, Japan or Carpintec CRC-15W, Ramsey, USA). The difference between the radioactivity in the injected and that in the killed animals was assumed to be due to excretion. Tumors and normal tissues of interest were dissected, rinsed to remove excess blood, weighed, and their radioactivity was measured using a γ-counter (LB2111, Berthold, Germany). The uptake in the tumor and healthy tissues of interest was calculated and expressed as a percentage of the injected radioactivity dose per gram of tissue. For blood, bone, muscle, and skin, total activity was estimated assuming that these organs constitute 6, 10, 40, and 15% of the total body weight, respectively. Urine was also collected and pooled together at the time the mice were killed.

In vivo stability

The stability of the complexes was assessed by analysis of urine and serum by RP-HPLC, under conditions identical to those used for analyzing the original radiopeptides. The samples were taken 1 h after injection. The urine collected at the time the mice were killed was filtered through a Millex GV filter (0.22 lm) before analysis. Blood collected from the mice was centrifuged at 3,000 rpm for 15 min at 4 °C, and the serum was separated. The serum was treated with ethanol in a 2:1 (v/v) ratio to precipitate the proteins. After centrifugation at 3,000 rpm for 15 min at 4 °C, the supernatant was collected and analyzed by RP-HPLC.

Results and discussion

Taking into consideration that the MC1R-binding affinity of bivalent ligands depends not only on the nature of the linkers between the targeting vectors, but also on the distance between those vectors [34, 35], we designed the two novel Boc-protected bifunctional chelators pz(Boc)$(CO_2H)_2$-A and pz(Boc)$(CO_2H)_2$-B, which contain a pyrazolyl-diamine chelating unit (N_3 donor atom set) for stabilization of the *fac*-$[M(CO)_3]^+$ core (M is ^{99m}Tc, Re) and two carboxylate groups for direct conjugation to the α-MSH analog NAPamide (Scheme 1).

Using these bifunctional chelators, with different overall architectures, we aimed at the selection of a lead construct with enhanced in vivo MC1R-targeting properties. The bifunctional chelator pz(Boc)$(CO_2H)_2$-A was synthesized starting with the precursor pz(Boc)(NH_2), whose preparation had already been described by our group (Scheme 1a) [39, 40]. The aza-Michael addition reaction of the primary amine in pz(Boc)(NH_2) with excess methyl acrylate gave a diester intermediate that upon hydrolysis in basic conditions gave pz(Boc)$(CO_2H)_2$-A in good overall yield (58%) [47].

The Boc-protected chelator pz(Boc)$(CO_2H)_2$-B was synthesized by alkaline hydrolysis of the precursor pz(Boc)$(CO_2H)(CO_2Et)$-B, which was prepared as previously described [41]. The compounds were characterized by the usual analytical chemistry techniques, including RP-HPLC, multinuclear NMR spectroscopy, and ESI–MS, as described in "Materials and methods." The homobivalent NAPamide conjugates $\mathbf{L^2}$ and $\mathbf{L^3}$ were prepared by conjugation of Pp-NAPamide to the bifunctional chelators pz(Boc)$(CO_2H)_2$-A and pz(Boc)$(CO_2H)_2$-B, respectively, using standard conjugation procedures (Scheme 2), and following the procedure previously described for $\mathbf{L^1}$ [17]. The conjugates were purified by semipreparative RP-HPLC and were characterized by ESI–MS (Table 1).

The synthesis of Pp-NAPamide started with the preparation of fully protected NAPamide by Fmoc-based solid-phase peptide synthesis in a CEM 12-channel automated peptide synthesizer, using a Sieber amide resin and the methyltrityl protecting group for the ε-amino group of Lys^{11}. Following simultaneous resin cleavage and selective removal of the methyltrityl group, and purification by RP-HPLC, Pp-NAPamide (greater than 95% purity) was characterized by ESI–MS (calculated *m/z* for $[M + H]^+$: 1,749.9; found: 1,750.0).

To evaluate the influence of metallation of $\mathbf{L^1}$–$\mathbf{L^3}$ on the MC1R-binding affinity and to characterize the radioactive complexes, we synthesized the "cold" rhenium complexes **1a**–**3a** by conjugation of the carboxylate groups in the precursors *fac*-$[Re(CO)_3(k^3$-pz$(CO_2H))]^+$, $[Re(CO)_3(k^3$-pz$(CO_2H)_2$-A$)]^+$, and *fac*-$[Re(CO)_3(k^3$-pz$(CO_2H)_2$-B$)]^+$ to the free ε-amino group of Lys^{11} of Pp-NAPamide, using standard coupling reagents (Scheme 3) [21]. The metallated peptides **1a**–**3a** were purified by semipreparative RP-HPLC and characterized by ESI–MS (Table 1).

The MC1R-binding affinity of the monovalent and bivalent conjugates $\mathbf{L^1}$–$\mathbf{L^3}$, as well as of the corresponding rhenium complexes (**1a**–**3a**), was assessed in a competitive binding assay using B16F1 murine melanoma cells and [^{125}I]NDP–MSH as a radioligand. The latter was prepared by radioiodination of NDP–MSH using the chloramine-T method as described in "Materials and methods." The radioiodinated product was purified by RP-HPLC before each assay to minimize the effect of deiodination of [^{125}I]NDP–MSH. The calculated IC_{50} values for all compounds are listed in Table 2, as are the IC_{50} values found for α-MSH, for the potent linear agonist NDP–MSH, and for the free NAPamide.

All compounds displayed high affinity for MC1R, with IC_{50} values in the subnanomolar and nanomolar range. The binding affinity of $\mathbf{L^1}$ ($IC_{50} = 0.66 \pm 0.13$ nM) is comparable to that of free NAPamide ($IC_{50} = 0.78 \pm 0.03$ nM), demonstrating that conjugation to the bifunctional chelator did not affect its original targeting

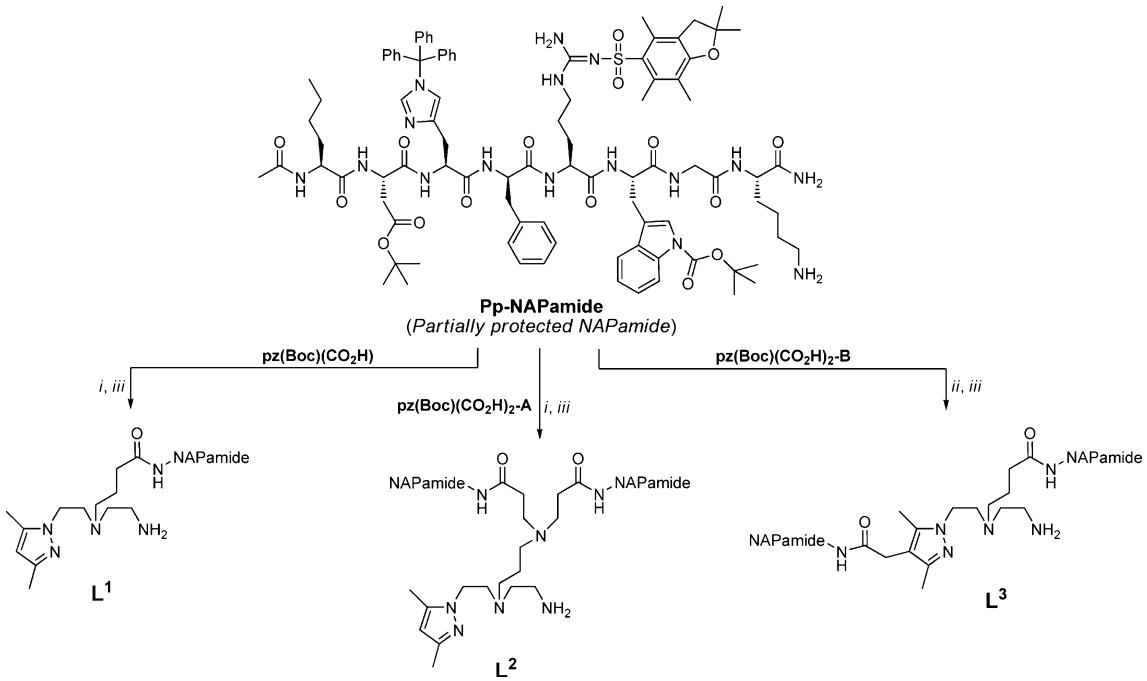

Scheme 2 *i* 2-(7-aza-1*H*-benzotriazole-1-yl)-1,1,3,3-tetramethyluronium hexafluorophosphate (HATU), *N*,*N*-diisopropylethylamine (DIPEA), dimethylformamide (DMF); *ii* HATU, DIPEA, microwave power 75 W, 50 °C, 10 min, DMF; *iii* 95% trifluoroacetic acid (TFA), 2.5% triisopropylsilane (TIS), 2.5% H_2O

Table 1 Analytical data for monovalent and bivalent α–melanocyte-stimulating hormone (α-MSH) derivatives and corresponding rhenium complexes

Compound	Formula	Calculated and ion	Found	t_R/min (purity)[a]
L^{1}	$C_{65}H_{96}N_{20}O_{12}$	1,349.8 $[M + H]^{+}$	1,349.8	14.1 (98%)
L^{2}	$C_{122}H_{177}N_{37}O_{24}$	849.5 $[M + 3H]^{3+}$	849.5	15.3 (98%)
L^{3}	$C_{119}H_{170}N_{36}O_{24}$	1,244.6 $[M + 2H]^{2+}$	1,244.6	15.0 (98%)
1a	$C_{68}H_{96}N_{20}O_{15}Re$	810.8 $[M + 2H]^{2+}$	810.4	15.9 (98%)
2a	$C_{125}H_{177}N_{37}O_{27}Re$	705.0 $[M + 3H]^{3+}$	705.0	15.4 (98%)
3a	$C_{122}H_{170}N_{36}O_{27}Re$	920.6 $[M + 3H]^{3+}$	920.6	15.5 (98%)

See Fig. 1 and Scheme 3 for the structures of the compounds

[a] The high-performance liquid chromatography conditions are described in "Materials and methods", Gradient D

properties. As envisaged, introduction of a second peptide unit in the same molecule resulted in a significant affinity enhancement. Indeed, the bivalent conjugates **L**^{2} ($IC_{50} = 0.035 \pm 0.018$ nM) and **L**^{3} ($IC_{50} = 0.16 \pm 0.21$ nM) had a 19-fold and fourfold increase in potency at the MC1R, respectively, compared with the monovalent peptide conjugate **L**^{1}. Metallation of the latter resulted in a 20-fold affinity enhancement (**1a**, $IC_{50} = 0.033 \pm 0.019$ nM), whereas a slight decrease in the binding affinity of **L**^{2} and **L**^{3} was observed upon metallation (**2a**, $IC_{50} = 0.15 \pm 0.08$ nM; **3a**, $IC_{50} = 1.14 \pm 1.13$ nM). Nevertheless, the values found for **2a** and **3a** are in the nanomolar range and are still better than or comparable to the value for NAPamide, suggesting that both compounds are potentially adequate for in vivo MC1R targeting.

Considering these promising results, we labeled both bivalent conjugates with ^{99m}Tc(I) following the method already described for **L**^{1} [17]. Reaction of **L**^{2} and **L**^{3} with the organometallic precursor *fac*-$[^{99m}Tc(CO)_3(H_2O)_3]^{+}$ gave the radiometallated peptides *fac*-$[^{99m}Tc(CO)_3(k^3\text{-L})]^{+}$ (**2**, L is **L**^{2}, and **3**, L is **L**^{3}) in high yield and high radiochemical purity. The chemical identity of the radiometallated peptides **2** and **3** was confirmed by comparing their RP-HPLC profiles with those of the corresponding rhenium

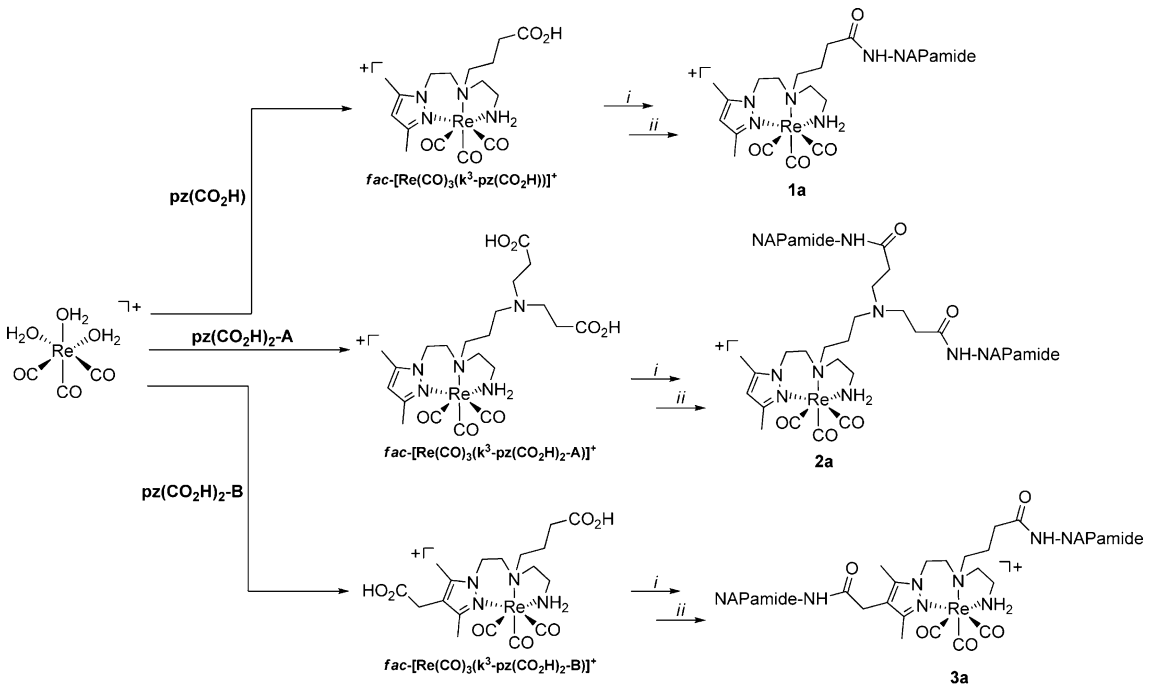

Scheme 3 Synthesis of complexes **1a**–**3a** containing pendant NAPamide targeting vectors. *i* Pp-NAPamide, DMF/DIPEA/HATU; *ii* TFA/TIS/H_2O

Table 2 Melanocortin type 1 receptor binding affinity of α-MSH derivatives

α-MSH derivatives	IC_{50} (nM)
α-MSH [46]	1.65 ± 0.18
NDP–MSH [48]	0.21 ± 0.03
NAPamide	0.78 ± 0.03
L^1	0.66 ± 0.13
L^2	0.035 ± 0.018
L^3	0.16 ± 0.21
1a	0.033 ± 0.019
2a	0.15 ± 0.08
3a	1.14 ± 1.13

NDP–MSH (Nle^4, D-Phe^7)–α-MSH, *NAPamide* [Ac-Nle^4, Asp^5, D-Phe^7, Lys_{11}]α-$MSH_{4–11}$

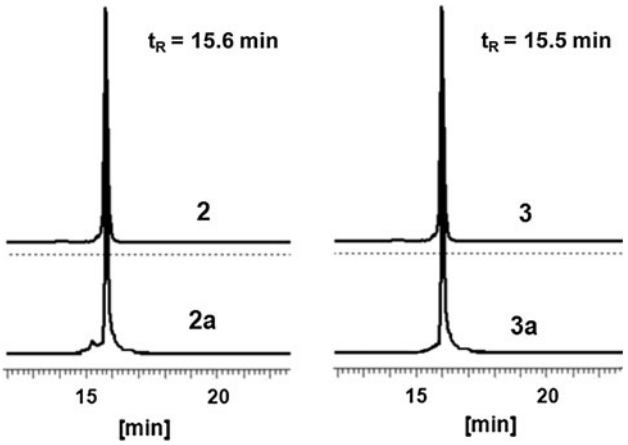

Fig. 2 Reversed-phase high-performance liquid chromatography (RP-HPLC) chromatograms of **2** and **3** (γ-detection) and **2a** and **3a** (UV–vis detection)

analogues **2a** and **3a**. RP-HPLC chromatograms of the metallated bivalent peptides **2/2a** and **3/3a** are displayed in Fig. 2. The overlapping profiles demonstrate the isostructural nature of the compounds prepared at the tracer (**2** and **3**) and macroscopic (**2a** and **3a**) levels.

The partition coefficients, expressed as log $P_{o/w}$, were determined for **2** and **3** in physiological conditions (Table 3). The results demonstrate the hydrophilic nature of all the radiometallated peptides, with complex **3** displaying the greatest hydrophilic character.

Radiopeptides **2** and **3** were incubated in fresh human serum at 37 °C, and aliquots were analyzed at different time points by RP-HPLC. The results showed that both compounds displayed high plasma stability with negligible degradation. As an illustrative example, Fig. 3 depicts the RP-HPLC chromatographic profile of **3** during the assay.

Complexes **2** and **3** are also stable in cysteine and histidine solutions since no degradation or *trans*-chelation products were observed even after 6 h incubation at 37 °C. Together, the stability studies confirmed the high ability of the pyrazolyl-diamine unit to stabilize the core *fac*-$[^{99m}Tc(CO)_3]^+$, without transmetallation to serum-based proteins or amino acids, and/or reoxidation to ^{99m}Tc(VII).

Table 3 Reversed-phase high-performance liquid chromatography retention times (t_R) and log $P_{o/w}$ values for complexes **1–3**

$^{99m}Tc(CO)_3$-labeled peptides	t_R (purity)	log $P_{o/w}$ ± SD
1 [17]	16.0 min (98%)	−0.420 ± 0.003
2	15.6 min (98%)	−1.34 ± 0.04
3	15.5 min (98%)	−1.82 ± 0.02

SD standard deviation

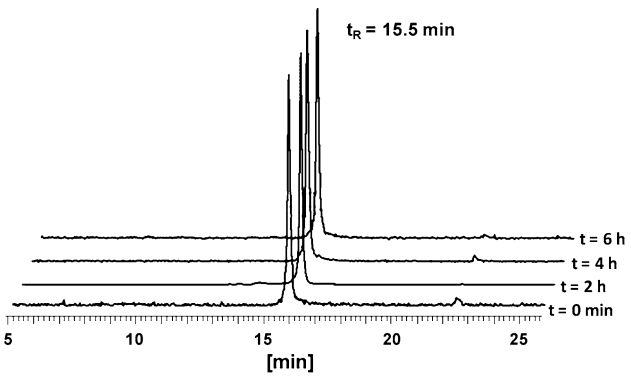

Fig. 3 RP-HPLC chromatograms of **3** after incubation in fresh human plasma at different time points

Internalization studies in B16F1 murine melanoma cells were performed for radioconjugates **2** and **3** at 37 °C, and the results were compared with those obtained for the monovalent radiopeptide **1** (Fig. 4a).

The cell uptake studies showed that the internalization degree is time-dependent, with bivalent radiopeptides **2** and **3** internalizing faster than **1** at short incubation times. Radiopeptide **2** had the highest level of internalization (9% of the total activity at 4 h incubation), whereas **3** displayed moderate internalization, with a pattern similar to that of the monovalent peptide **1** (about 5% of the applied activity at 4 h incubation).

To check whether the cellular internalization was specific and receptor-mediated, the bivalent radiocomplexes were also incubated in the presence of a high concentration of NDP–MSH to block the MC1Rs. The results of receptor blockade, expressed as a percentage of internalization in the presence and in the absence of NDP–MSH, are displayed in Fig. 5.

Co-incubation with excess NDP–MSH, a potent MC1R agonist, reduced significantly the cellular internalization of **2** and **3** by 70–76% and 50–56%, respectively. These data indicate that both radiocomplexes are taken up by melanoma cells through an MC1R-mediated mechanism.

Cellular retention of **2** and **3** was also evaluated in B16F1 cells at different time points and compared with the results previously described for **1** (Fig. 4b). After 4 h incubation, **2** had a retention value higher than that of **3** (52 and 40% of the total activity is associated with cells, respectively). However, the monovalent radiopeptide (**1**) had the highest cell-associated radioactivity value (62%, after 4 h incubation) [17].

The internalization and cellular retention studies in B16F1 cells for all the radiolabeled peptides reflect agonistic binding behavior, which is consistent with data previously reported for other radiolabeled α-MSH analogs [16].

The in vivo MC1R-targeting properties of **2** and **3** were also evaluated in B16F1 melanoma-bearing mice. Table 4 presents the tissue distributions of **2** and **3** in comparison with radiopeptide **1** at 1 and 4 h after injection of the radiopeptide.

The analysis of blood samples collected from the killed mice at 1 h after injection showed that **2** and **3** are stable in blood serum, as no metabolites could be detected (Fig. 6). The low stomach uptake observed for all the radiopeptides

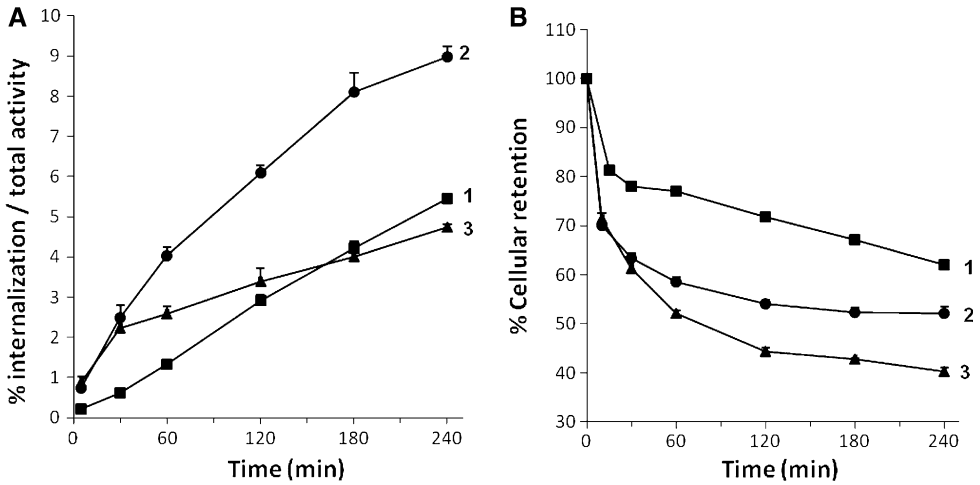

Fig. 4 Internalization (**a**) and retention (**b**) of **1** (*squares*), **2** (*circles*), and **3** (*triangles*) in B16F1 cells at 37 °C. Internalized activity is expressed as a percentage of the total (applied) activity

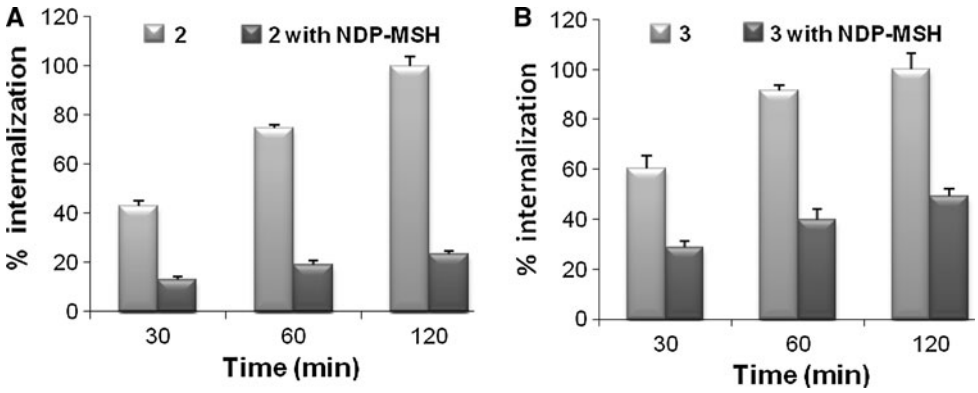

Fig. 5 Receptor-blocking study: inhibition of cellular internalization of **2** (**a**) and **3** (**b**) in B16F1 cells by co-incubation with (Nle^4, D-Phe^7)–α-MSH (*NDP-MSH*) (3.5 μg per well)

Table 4 Biodistribution studies of **1**–**3** in B16F1 melanoma-bearing C57BL/6 mice at 1 and 4 h after injection ($n = 3$–5)

Organ	**1**		**2**		**3**	
	1 h	4 h	1 h	4 h	1 h	4 h
% ID/g ± SD						
Tumor	5.88 ± 2.11	4.24 ± 0.94	3.02 ± 0.27	2.96 ± 0.36	2.54 ± 0.30	1.81 ± 0.44
Blood	3.32 ± 0.51	1.62 ± 0.64	1.36 ± 0.30	0.62 ± 0.06	2.39 ± 0.61	0.49 ± 0.13
Liver	10.8 ± 1.6	6.7 ± 2.1	45.7 ± 7.1	35.3 ± 5.97	21.3 ± 0.2	10.1 ± 2.2
Intestine	9.1 ± 0.8	14.4 ± 1.6	2.75 ± 0.25	4.57 ± 1.05	1.78 ± 0.02	2.82 ± 1.29
Spleen	1.26 ± 0.2	0.88 ± 0.30	1.80 ± 0.09	2.16 ± 1.01	3.12 ± 0.58	1.52 ± 0.42
Heart	0.85 ± 0.1	0.58 ± 0.19	0.63 ± 0.14	0.39 ± 0.03	1.01 ± 0.08	0.39 ± 0.14
Lungs	2.88 ± 0.55	1.21 ± 0.45	1.34 ± 0.14	0.67 ± 0.08	3.66 ± 0.50	0.60 ± 0.10
Kidney	9.7 ± 0.9	4.5 ± 2.4	33.2 ± 3.3	36.8 ± 3.87	68.6 ± 6.4	72.5 ± 1.1
Muscle	0.31 ± 0.03	0.18 ± 0.14	0.24 ± 0.01	0.07 ± 0.08	0.33 ± 0.03	0.1 ± 0.02
Bone	0.66 ± 0.10	0.40 ± 0.20	0.61 ± 0.03	0.40 ± 0.00	0.72 ± 0.07	0.31 ± 0.06
Stomach	2.92 ± 1.70	1.06 ± 0.96	1.18 ± 0.62	0.38 ± 0.04	0.88 ± 0.30	0.33 ± 0.14
Pancreas	0.57 ± 0.10	0.46 ± 0.32	0.31 ± 0.05	0.20 ± 0.04	0.40 ± 0.02	0.43 ± 0.41
Tumor/normal tissue uptake ratio						
Tumor/blood	1.8	2.6	2.2	4.8	1.1	3.7
Tumor/muscle	19.0	23.5	12.6	42.3	7.7	18.1
Tumor/kidney	0.60	0.94	0.09	0.08	0.037	0.025
Total excretion (%)	57.3 ± 2.7	69.1 ± 8.3	21.6 ± 1.6	32.0 ± 2.8	39.9 ± 6.4	51.9 ± 1.8

ID injected dose

indicates minimal, if any, in vivo oxidation of the complexes to $[^{99m}TcO_4]^-$, revealing the high kinetic inertness of the radioactive complexes. A small amount (less than 15%) of metabolites with a shorter retention time were found in urine but they were not identified.

The bivalent radiopeptides **2** and **3** showed lower tumor uptake and worse pharmacokinetic properties than the monovalent radiopeptide **1**. Slower overall excretion was observed for both bivalent radiopeptides when compared with **1**, with **2** displaying the worst value, with only 32.0 ± 2.8% of the activity excreted at 4 h after injection. Radiopeptides **2** and **3** were rapidly cleared from the bloodstream [0.62 ± 0.06 and 0.49 ± 0.13% injected dose (ID) per gram at 4 h after injection] and major organs, except those related to the excretion pathways.

As predicted from their in vitro potency, the metallated NAPamide derivatives with the highest in vitro binding affinity displayed the highest in vivo melanoma accumulation. Indeed, the ranking of melanoma uptake for the radiopeptides (4.24, 2.96, and 1.81% ID/g at 4 h after injection for **1**, **2**, and **3**, respectively) correlates well with the in vitro MC1R-binding affinity of the respective "cold" surrogates (IC_{50} values of 0.033, 0.15, and 1.14 nM for **1a**, **2a**, and **3a**, respectively; Table 2).

The findings of the cell internalization studies do not correlate with the in vivo targeting properties of both

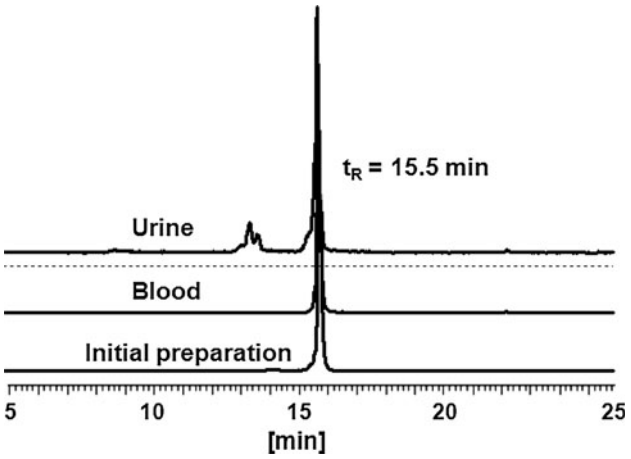

Fig. 6 RP-HPLC γ traces of **3** (initial preparation), blood serum, and urine samples collected 1 h after injection

bivalent constructs. Indeed, the highest cell internalization level and the moderate retention observed for **2**, together with its nanomolar MC1R-binding affinity, did not lead to an enhancement of tumor uptake relative to **1**. In fact, there was not a positive correlation between the tumor uptake and the number of targeting vectors on the complexes, which may be partially explained by the poor tissue penetration of **2** in vivo.

In spite of the low tumor uptake observed, **2** displayed the highest tumor retention as 98% of the radioactivity measured at 1 h was still retained in the tumor after 4 h. These results partially account for the best tumor-to-blood and tumor-to-muscle ratios at 4 h after injection found for **2**.

Unlike **1**, both bivalent radiopeptides showed very high nonspecific accumulation and retention in kidneys (33.2 ± 3.3 and 36.8 ± 3.87% ID/g for **2** and 68.6 ± 6.4 and 72.5 ± 1.1% ID/g for **3** at 1 and 4 h after injection, respectively). These results, often reported for other radiopeptides, are indicative of pronounced tubular reabsorption, which is likely related to the binding to the multiligand megalin receptor [16, 26, 37, 49–51]. Whether nonspecific uptake by kidneys could have been modulated (e.g., by infusion of basic amino acids) was not studied. The high kidney uptake and retention, together with the low tumor uptake led to poor tumor-to-kidney ratios (e.g., 0.08 and 0.025 for **2** and **3**, respectively, at 4 h after injection), which are considerably lower than the ratio obtained for the monovalent compound **1** (e.g., 0.94 at 4 h after injection). This behavior is comparable to that reported for other radiolabeled bivalent α-MSH and multivalent RGD derivatives [26, 37]. In the former case, the tumor-to-kidney ratios observed for three bivalent ^{111}In-DOTA-labeled NAPamide analogs ranged between 0.11 and 0.36, which are also considerably lower than the ratio observed for the monovalent ^{111}In-DOTA-NAPamide (1.67) [37].

Concluding remarks and perspectives

We have applied the multivalency concept to the design of novel homobivalent conjugates containing a pyrazolyl-diamine chelating unit for stabilization of the *fac*-$[M(CO)_3]^+$ core (M is ^{99m}Tc, Re) and two copies of the targeting vector NAPamide, a linear α-MSH analog, separated by linkers of different nature ($\mathbf{L^2}$, symmetric alkyl chain; $\mathbf{L^3}$, "asymmetric" "semirigid" spacer) and length ($\mathbf{L^2}$, nine atoms; $\mathbf{L^3}$, 14 atoms). The in vitro MC1R-binding affinity of the bivalent conjugates was found to be 19-fold ($\mathbf{L^2}$) and fourfold ($\mathbf{L^3}$) higher than that of the monovalent NAPamide conjugate ($\mathbf{L^1}$). Metallation of the bivalent conjugates yielded isostructural complexes of the type [*fac*-$M(CO)_3(k^3$-L)] (M is ^{99m}Tc/Re; **1/1a**, L is $\mathbf{L^1}$; **2/2a**, L is $\mathbf{L^2}$; **3/3a**, L is $\mathbf{L^3}$), with **2a** and **3a** displaying binding affinities in the subnanomolar and nanomolar range, which are still better than (**2a**, $IC_{50} = 0.15 \pm 0.08$ nM) or comparable to (**3a**, $IC_{50} = 1.14 \pm 1.13$ nM) the binding affinity of NAPamide ($IC_{50} = 0.78 \pm 0.03$ nM). Cell internalization studies in B16F1 murine melanoma cells have shown that the analog radiopeptides **2** and **3** internalize via an MC1R-mediated mechanism faster than **1** at short times, with **2** having the highest level of internalization. The biodistribution studies in B16F1 melanoma-bearing mice have shown that melanoma uptake (4.24, 2.96, and 1.81% ID/g at 4 h after injection for **1**, **2**, and **3**, respectively) correlates well with the in vitro MC1R-binding affinity of the rhenium surrogates (**1a**, $IC_{50} = 0.033$ nM; **2a**, $IC_{50} = 0.15$ nM; **3a**, $IC_{50} = 1.14$ nM). However, there is no positive correlation between tumor uptake and valency, even in the case of **2**, which had the highest cellular internalization level and better retention. This behavior is most likely related to the poor tissue penetration of **2**. Nevertheless, **2** displayed the highest level of tumor retention, as 98% of the radioactivity measured at 1 h was still retained after 4 h, which partially accounts for its best tumor-to-blood and tumor-to-muscle ratios at 4 h after injection. Additionally, one striking feature observed for both radiopeptides is the remarkable increase in nonspecific kidney accumulation and retention, which led to low tumor-to-kidney ratios for the bivalent compounds. Such behavior has been already reported for other radiolabeled bivalent α-MSH and multivalent RGD derivatives. Together, the results have demonstrated that the high in vitro MC1R-binding affinity and the high level of cellular internalization/retention observed for ^{99m}Tc$(CO)_3$-labeled bivalent NAPamide conjugates did not lead to increased tumor uptake and improved pharmacokinetic profile

relative to the monovalent counterpart. Indeed, there is no positive correlation between tumor uptake and valency. Nevertheless, to take advantage of the favorable in vitro MC1R-targeting properties and in vivo tumor retention of radiopeptide **2**, improvement of its pharmacokinetic profile by modifying the charge and/or nature of the metal chelator/spacer is envisaged.

Acknowledgments M.M. thanks the Fundação para a Ciência e Tecnologia (FCT) for a PhD fellowship (SFRH/BD/48066/2008). Covidean-Mallinckrodt is acknowledged for the IsoLink® kits. J. Marçalo is acknowledged for performing the ESI–MS analyses. The electrospray ionization quadrupole ion trap mass spectrometer was acquired with the support of the Programa Nacional de Reequipamento Científico of FCT and which is part of RNEM-Rede Nacional de Espectrometria de Massa, also supported by FCT.

References

1. Correia JD, Paulo A, Raposinho PD, Santos I (2011) Dalton Trans 40:6144–6167. doi:10.1039/c0dt01599g
2. Reubi JC, Maecke HR (2008) J Nucl Med 49:1735–1738. doi:10.2967/jnumed.108.053041
3. Lee S, Xie J, Chen X (2010) Biochemistry 49:1364–1376. doi:10.1021/bi901135x
4. Gray-Schopfer V, Wellbrock C, Marais R (2007) Nature 445:851–857. doi:10.1038/nature05661
5. Carlson JA, Slominski A, Linette GP, Mihm MC Jr, Ross JS (2003) Expert Rev Mol Diagn 3:303–330. doi:10.1586/14737159.3.3.303
6. Carlson JA, Slominski A, Linette GP, Mihm MC Jr, Ross JS (2003) Expert Rev Mol Diagn 3:163–184. doi:10.1586/14737159.3.2.163
7. Jemal A, Siegel R, Ward E, Hao Y, Xu J, Thun MJ (2009) CA Cancer J Clin 59:225–249. doi:10.3322/caac.20006
8. Miao Y, Quinn TP (2008) Crit Rev Oncol Hematol 67:213–228. doi:10.1016/j.critrevonc.2008.02.006
9. Wei L, Zhang X, Gallazzi F, Miao Y, Jin X, Brechbiel MW, Xu H, Clifford T, Welch MJ, Lewis JS, Quinn TP (2009) Nucl Med Biol 36:345–354. doi:10.1016/j.nucmedbio.2009.01.007
10. Quinn T, Zhang X, Miao Y (2010) G Ital Dermatol Venereol 145:245–258
11. Eberle AN, Froidevaux S (2003) J Mol Recognit 16:248–254. doi:10.1002/jmr.633
12. Froidevaux S, Calame-Christe M, Schuhmacher J, Tanner H, Saffrich R, Henze M, Eberle AN (2004) J Nucl Med 45:116–123
13. Cheng Z, Zhang L, Graves E, Xiong Z, Dandekar M, Chen X, Gambhir SS (2007) J Nucl Med 48:987–994. doi:10.2967/jnumed.107.039602
14. Cheng Z, Xiong Z, Subbarayan M, Chen X, Gambhir SS (2007) Bioconjug Chem 18:765–772. doi:10.1021/bc060306g
15. Ren G, Liu Z, Miao Z, Liu H, Subbarayan M, Chin FT, Zhang L, Gambhir SS, Cheng Z (2009) J Nucl Med 50:1865–1872. doi:10.2967/jnumed.109.062877
16. Raposinho PD, Xavier C, Correia JDG, Falcao S, Gomes P, Santos I (2008) J Biol Inorg Chem 13:449–459. doi:10.1007/s00775-007-0338-3
17. Raposinho PD, Correia JDG, Alves S, Botelho MF, Santos AC, Santos I (2008) Nucl Med Biol 35:91–99. doi:10.1016/j.nucmedbio.2007.08.001
18. Raposinho PD, Correia JDG, Oliveira MC, Santos I (2010) Biopolymers 94:820–829. doi:10.1002/bip.21490
19. Haskell-Luevano C, Todorovic A, Gridley K, Sorenson N, Irani B, Xiang Z (2004) Endocr Res 30:591–597
20. Holder JR, Haskell-Luevano C (2004) Med Res Rev 24:325–356. doi:10.1002/med.10064
21. Garcia-Borron JC, Sanchez-Laorden BL, Jimenez-Cervantes C (2005) Pigment Cell Res 18:393–410. doi:10.1111/j.1600-0749.2005.00278.x
22. Eberle AN, Bapst JP, Calame M, Tanner H, Froidevaux S (2010) Adv Exp Med Biol 681:133–142. doi:10.1007/978-1-4419-6354-3_11
23. Abiraj K, Jaccard H, Kretzschmar M, Helm L, Maecke HR (2008) Chem Commun 3248–3250. doi:10.1039/b805281f
24. Liu S (2006) Mol Pharm 3:472–487. doi:10.1021/mp060049x
25. Kiessling LL, Gestwicki JE, Strong LE (2006) Angew Chem Int Ed 45:2348–2368. doi:10.1002/anie.200502794
26. Singh AN, Liu W, Hao G, Kumar A, Gupta A, Oz OK, Hsieh JT, Sun X (2011) Bioconjug Chem 22:1650–1662. doi:10.1021/bc200227d
27. Shi J, Wang L, Kim YS, Zhai S, Jia B, Wang F, Liu S (2009) Eur J Nucl Med Mol Imaging 36:1874–1884. doi:10.1007/s00259-009-1166-1
28. Liu W, Hao G, Long MA, Anthony T, Hsieh JT, Sun X (2009) Angew Chem Int Ed 48:7346–7349. doi:10.1002/anie.200903556
29. Almutairi A, Rossin R, Shokeen M, Hagooly A, Ananth A, Capoccia B, Guillaudeu S, Abendschein D, Anderson CJ, Welch MJ, Frechet JM (2009) Proc Natl Acad Sci USA 106:685–690. doi:10.1073/pnas.0811757106
30. Montet X, Funovics M, Montet-Abou K, Weissleder R, Josephson L (2006) J Med Chem 49:6087–6093. doi:10.1021/jm060515m
31. Dijkgraaf I, Kruijtzer JA, Liu S, Soede AC, Oyen WJ, Corstens FH, Liskamp RM, Boerman OC (2007) Eur J Nucl Med Mol Imaging 34:267–273. doi:10.1007/s00259-006-0180-9
32. Eberle A, Kriwaczek VM, Schwyzer R (1977) FEBS Lett 80:246–250
33. Kriwaczek VM, Eberle AN, Muller M, Schwyzer R (1978) Helv Chim Acta 61:1232–1240
34. Vagner J, Handl HL, Monguchi Y, Jana U, Begay LJ, Mash EA, Hruby VJ, Gillies RJ (2006) Bioconjug Chem 17:1545–1550. doi:10.1021/bc060154p
35. Handl HL, Sankaranarayanan R, Josan JS, Vagner J, Mash EA, Gillies RJ, Hruby VJ (2007) Bioconjug Chem 18:1101–1109. doi:10.1021/bc0603642
36. Bagutti C, Stolz B, Albert R, Bruns C, Pless J, Eberle AN (1994) Int J Cancer 58:749–755
37. Bapst JP, Froidevaux S, Calame M, Tanner H, Eberle AN (2007) J Recept Signal Transduct Res 27:383–409. doi:10.1080/10799890701723528
38. Santos I, Alves S, Paulo A, Correia JDG, Gano L, Smith CJ, Hoffman TJ (2005) Bioconjug Chem 16:438–449. doi:10.1021/bc0497968
39. Oliveira BL, Raposinho PD, Mendes F, Figueira F, Santos I, Ferreira A, Cordeiro C, Freire AP, Correia JDG (2010) Bioconjug Chem 21:2168–2172. doi:10.1021/bc100291e
40. Oliveira BL, Raposinho PD, Mendes F, Santos IC, Santos I, Ferreira A, Cordeiro C, Freire AP, Correia JDG (2011) J Organomet Chem 696:1057–1065. doi:10.1016/j.jorganchem.2010.09.019
41. Esteves T, Marques F, Paulo A, Rino J, Nanda P, Smith CJ, Santos I (2011) J Biol Inorg Chem. doi:10.1007/s00775-011-0803-x
42. Alberto R, Ortner K, Wheatley N, Schibli R, Schubiger AP (2001) J Am Chem Soc 123:3135–3136
43. Zubieta J, Lazarova N, James S, Babich J (2004) Inorg Chem Commun 7:1023–1026. doi:10.1016/j.inoche.2004.07.006
44. Palma E, Oliveira BL, Correia JD, Gano L, Maria L, Santos IC, Santos I (2007) J Biol Inorg Chem 12:667–679. doi:10.1007/s00775-007-0215-0

45. Troutner DE, Volkert WA, Hoffman TJ, Holmes RA (1984) Int J Appl Radiat Isot 35:467–470
46. Froidevaux S, Calame-Christe M, Tanner H, Eberle AN (2005) J Nucl Med 46:887–895
47. Long TE, Mather BD, Viswanathan K, Miller KM (2006) Prog Polym Sci 31:487–531. doi:10.1016/j.progpolymsci.2006.03.001
48. Quinn TP, Chen JQ, Cheng Z, Owen NK, Hoffman TJ, Miao YB, Jurisson SS (2001) J Nucl Med 42:1847–1855
49. Bapst JP, Calame M, Tanner H, Eberle AN (2009) Bioconjug Chem 20:984–993. doi:10.1021/bc900007u
50. de Jong M, Barone R, Krenning E, Bernard B, Melis M, Visser T, Gekle M, Willnow TE, Walrand S, Jamar F, Pauwels S (2005) J Nucl Med 46:1696–1700
51. Verroust PJ, Christensen EI (2002) Nephrol Dial Transplant 17:1867–1871